AIAA 81-1226R

Mach 6 Experiments of Transition on a Cone at Angle of Attack

Kenneth F. Stetson*
Air Force Wright Aeronautical Laboratories, Wright Patterson Air Force Base, Ohio

Transition movement and patterns on the frustum of a cone at small angles of attack have been investigated at a Mach number of 5.9, using an 8-deg half-angle cone with both sharp and blunt nosetips. Small angles of attack produced large asymmetries in the frustum transition pattern for both sharp and blunt tipped configurations. For the configurations with nosetip bluntness most of the frustum transition asymmetry occurred between meridian angles of 60 and 120 deg. Data obtained with simulated laminar ablated nosetips were generally representative of what would be expected with a larger spherically blunt nosetip.

Nomenclature

B = beginning of transition
E = end of transition
L = leeward side
M = Mach number
R_B = model base radius
R_N = model nosetip radius
Re = Reynolds number
Re_x = Reynolds number based upon conditions at the edge of the boundary layer and surface distance from the sharp tip or stagnation point
Re_θ = Reynolds number based upon conditions at the edge of the boundary layer and the laminar boundary-layer momentum thickness
X = surface distance (except Fig. 1), in.
X_T = surface distance from the sharp tip or stagnation point to the onset of transition, in.
T = temperature, R
W = windward
α = angle of attack, deg
θ_c = cone half-angle, deg
ϕ = cone meridian angle, deg

Subscripts

s = sharp
∞ = freestream
w = model surface
0 = reservoir

Introduction

INTUITION derived from boundary-layer transition results at zero angle of attack is not very helpful in predicting the transition trends on a sharp cone at angle of attack. The effect of angle of attack is to increase the local Reynolds number and decrease the local Mach number on the windward ray. One might logically assume that transition would then move forward on the windward ray with increases in angle of attack. On the leeward ray the local Reynolds number decreases and the local Mach number increases. Based upon results obtained at zero angle of attack, it might be expected that transition would move rearward on the leeward ray with increases in angle of attack. In reality, just the opposite of these trends occur. Transition experiments[1-9] with a sharp cone have consistently found a rearward movement of transition on the windward ray and a forward movement on the leeward ray. These trends are also supported by boundary-layer stability theory.[10] Moore's[10] results show that the boundary-layer profiles assume a more stable shape on the windward side and a more unstable shape on the leeward side.

Hypersonic nosetip bluntness investigations[6-9] have demonstrated the strong influence of the nosetip on the location of frustum transition. A question which has received little consideration is the effect of nosetip shape on frustum transition. Historically laboratory experiments have been performed with conical frustrums and spherically blunt nosetips. Nonspherical nosetips have important applications, for example, for hypersonic re-entry vehicles. The nosetip of such a vehicle would normally be expected to experience ablation under laminar boundary-layer heating conditions, and obtain a nonspherical configuration, before transition occurs on the frustum. The effect of this nosetip configuration change on frustum transition location and transition asymmetries is not known. A brief look at this problem was made by conducting transition experiments with a nosetip configuration which simulated a spherical nosetip which had experienced laminar ablation. The configuration selected was not meant to simulate any particular set of flight and nosetip material conditions, but only to be representative of the class of configurations resulting from laminar ablation.

The literature contains only limited data on the effects of angle of attack on boundary-layer transition. Most of the available results are for a sharp cone and usually contain only data on the windward and leeward rays. The data base is

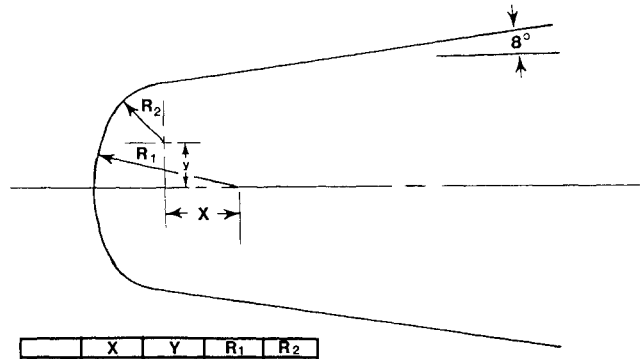

	X	Y	R_1	R_2
5%L	.073	.043	.140	.056
10%L	.146	.086	.280	.112
15%L	.219	.129	.420	.168

Fig. 1 Simulated laminar ablated nosetip configurations.

Presented as Paper 81-1226 at the AIAA 14th Fluid and Plasma Dynamics Conference, Palo Alto, Calif., June 23-25, 1981; submitted July 13, 1981; revision received Feb. 11, 1982.

*Aerospace Engineer, High Speed Aero-Performance Branch, Aeromechanics Division, Flight Dynamics Laboratory. Associate Fellow AIAA.

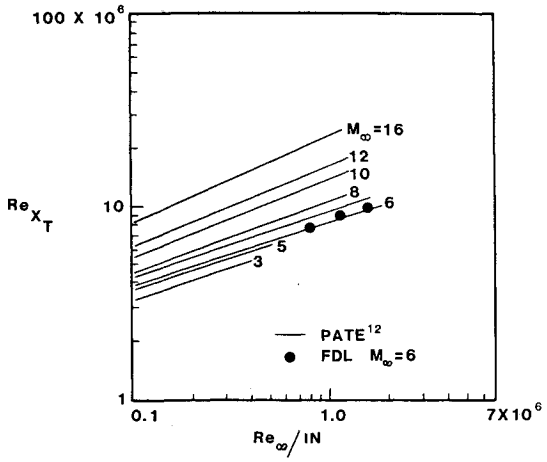

Fig. 2 Effect of Mach number and unit Reynolds number on sharp cone transition for small size wind tunnels (Re_{X_T} is the end of transition).

SHARP CONE

CURVE NO.	SOURCE	θ_c	M_∞	FACILITY	TECHNIQUE
1	DICRISTINA	8°	10	WIND TUNNEL	SHADOW GRAPH
2	WARD	10°	5	WIND TUNNEL	SHADOW GRAPH
3	HOLDEN	6°	13.3	SHOCK TUNNEL	HEAT TRANSFER SCHLIEREN
4	KROGMANN	5°	5	LUDWIEG TUBE	SURFACE HEAT TRANSFER
5	STETSON RUSHTON	8°	5.5	SHOCK TUNNEL	SURFACE HEAT TRANSFER
• ---	PRESENT DATA	8°	5.9	WIND TUNNEL	SURFACE HEAT TRANSFER

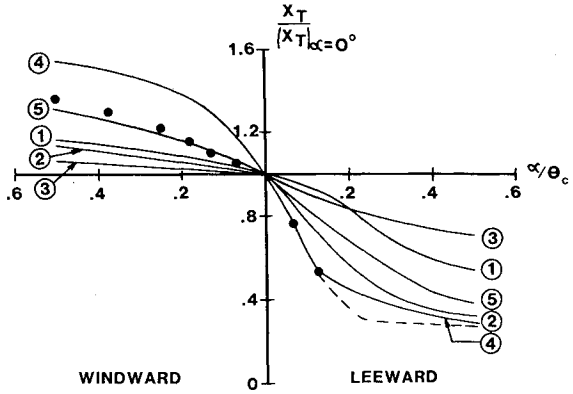

Fig. 3 Comparison of the movement of transition on a sharp cone at angle of attack.

inadequate to confidently model the circumferential transition pattern on a blunt cone at angle of attack. The primary objective of the present program was to measure the asymmetric transition patterns which developed on sharp and blunt cones at small angles of attack. All results were obtained on an 8-deg half-angle cone at a freestream Mach number of 5.9.

Experimental Apparatus and Procedures

The experiments were conducted in the FDL Mach 6 wind tunnel. This tunnel is a blowdown facility operating at a reservoir temperature of 1100 R and a reservoir pressure range of 700 to 2100 psia, corresponding to a Reynolds number per foot range of 9.7 to 30.3×10^6. The test core of approximately 10 in. is produced by a contoured axisymmetric nozzle with a physical exit diameter of 12.3 in. Additional details of the tunnel can be found in Ref. 11. The test model was a thin-skin (nominally 0.025 in.), 8-deg half-angle cone containing two rays of thermocouples. The base diameter of the model was 4 in. and the model had, in addition to a sharp tip, spherically blunt nosetips with the following bluntness ratios: $R_N/R_B = 0.02$, 0.05, 0.10, and 0.15. The dimensions of the three nosetips utilized in the simulated laminar ablated nosetip experiments are given in Fig. 1 and are designated as 5%L, 10%L and 15%L. These nosetips correspond to 5%, 10%, and 15% spherically blunt nosetips which have experienced laminar ablation. Nominal model surface finish was 15 μ in.and the blunt nosetips were polished before each run. The model was cooled between runs so that the model surface temperature would always be the same at the start of each run (approximately 540 R). The location of boundary-layer transition was obtained from heat transfer measurements. Heat transfer rates were calculated from the increase in the surface temperature of the model, during a time interval of 0.5 s, after the model arrived at the tunnel centerline. T_w/T_0 was generally in the range of 0.52-0.58.

For this series of experiments the model had two rays of thermocouples and circumferential patterns were obtained by rolling the model and making repeat runs. Test conditions could be duplicated very closely and the transition location for a given situation could be closely reproduced, as evidenced by the close agreement of many repeat runs. Transition patterns were obtained by making a composite picture from the results of several runs.

Sharp cone transition data were compared with the correlation of Pate.[12] Pate made an extensive study of the relationship between wind tunnel freestream disturbances and boundary-layer transition and developed a method to predict boundary-layer transition in wind tunnels with Mach number,

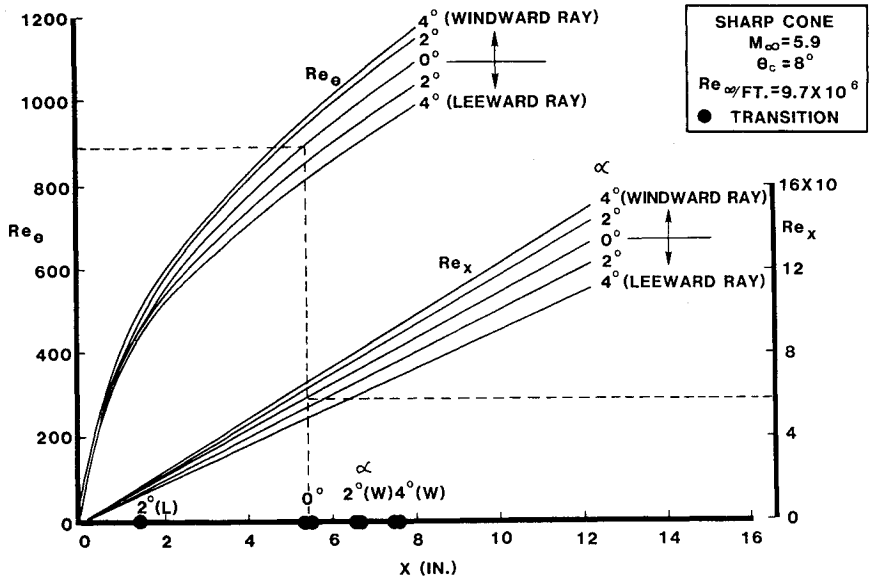

Fig. 4 Local Reynolds number calculations for a sharp cone at angle of attack.

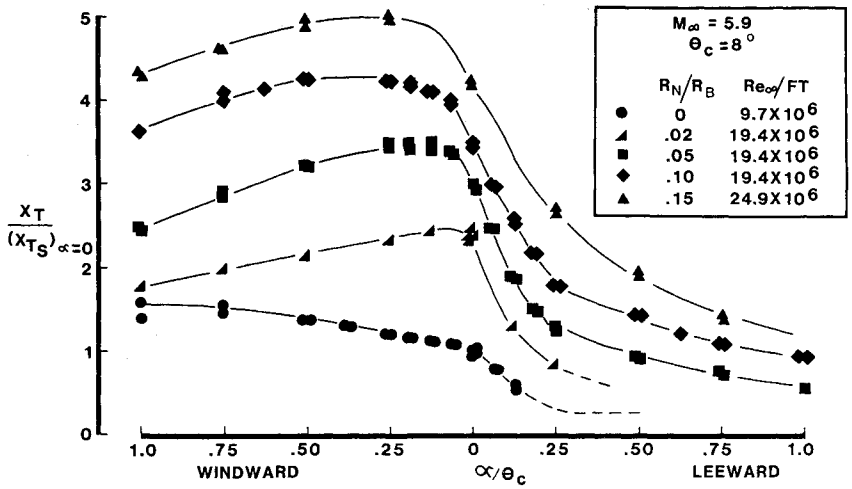

Fig. 5 Transition movement with angle of attack.

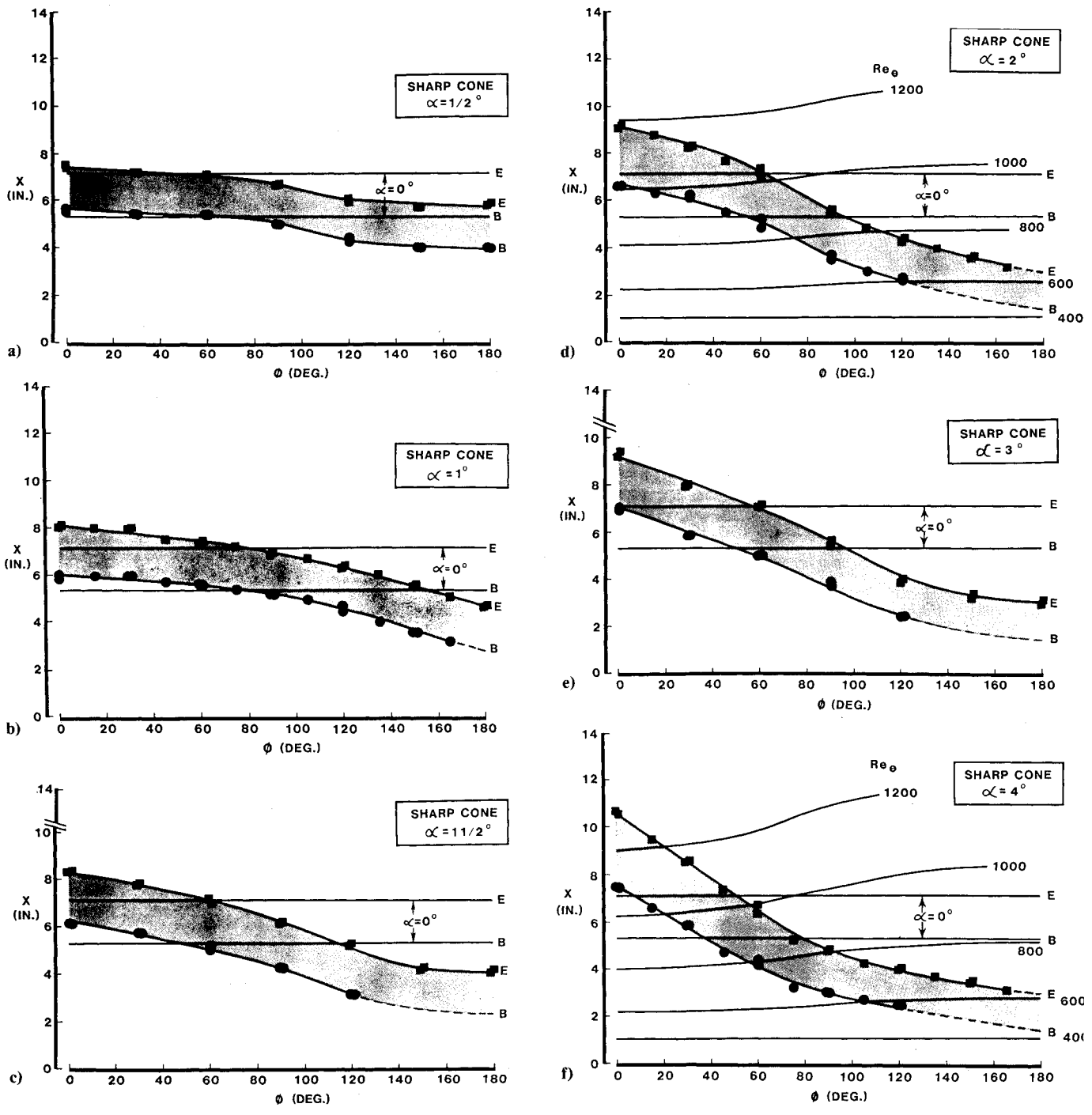

Fig. 6 Transition pattern on a sharp cone, a) $\alpha = 0.5$ deg, b) $\alpha = 1$ deg, c) $\alpha = 1.5$ deg, d) $\alpha = 2$ deg, e) $\alpha = 3$ deg, f) $\alpha = 4$ deg.

unit Reynolds number, and tunnel size as parameters. Figure 2 indicates Pate's predictions for the end of boundary-layer transition on sharp cones at zero angle of attack in small size wind tunnels. The excellent agreement of these present transition data with the results of Pate indicated that boundary-layer transition in the FDL tunnel is influenced by aerodynamic noise in a predictable manner, similar to the 17 wind tunnels considered by Pate. Furthermore, since the occurrence of transition on a wind tunnel model is the result of the combined effect of all disturbance parameters, such as freestream disturbances, model surface roughness, model vibration, flow angularity, etc.; the fact that transition Reynolds numbers were found to be the same in several wind tunnels would infer a similarity in the influence of the combined effect of disturbance parameters on boundary-layer transition. Additional details of transition comparisons with other facilities and transition results obtained in the FDL $M=6$ wind tunnel can be found in Ref. 9.

Results

A good starting point is to compare these new angle-of-attack transition data with other available data. This is done for the windward and leeward meridians of a sharp cone, since this is the situation where the largest variety of data exists. This comparison is made in Fig. 3. Additional data are available; however, the five references selected were believed to be a good cross section of available data, containing results from different facilities, and for a variety of cone angles and flow Mach numbers. The general trend of a rearward movement of transition on the windward ray and a forward movement on the leeward ray is found for all of these data. However, significant differences in the magnitude of this displacement are found. There does not appear to be sufficient data available to distinguish any trends associated with cone angle, Mach number, type of facility, or measurement technique. This is not meant to imply that such trends do not exist, only that at present there is insufficient data to make such an evaluation. Therefore the "correct" magnitude of transition displacement with angle of attack is unknown. These present results are believed to be compatible with previous results; however, the author is unable to explain or predict the magnitude of displacement for either the new or old data.

Figure 4 presents results of local Reynolds number calculations for a sharp, 8-deg half-angle cone at angle of attack using a boundary-layer code developed by Hecht et al.[13] which is based upon integral solutions of the boundary-layer equations. Also shown are the locations of transition obtained from these experiments. Comparison of the experimental transition locations with the calculated Reynolds numbers provide local transition Reynolds number. The local transition Reynolds number increased on the windward ray and decreased on the leeward ray as the angle of attack was increased.

Figure 5 illustrates the transition movement on the windward and leeward rays of sharp and blunt 8-deg half-angle cones. The transition distance (X_T) is normalized by the transition distance on the sharp cone at $\alpha=0$ deg [$(X_{T_S})_{\alpha=0}$ varies with unit Reynolds number]. The 15% blunt nosetip was tested at a slightly larger unit Reynolds number than the other blunt configurations to keep transition from moving off the end of the model at $\alpha=2$ deg. The sharp cone transition trends were consistent with expected results, as noted earlier. The blunt configurations, however, have trends which are somewhat different from those of Ref. 7. These differences relate to the windward ray at small angles of attack. Reference 7 had the maximum rearward displacement at $\alpha=0$ deg and a forward movement with angle of attack. The present data consistently had a rearward movement initially, as for the sharp cone, and then a forward movement at larger angles of attack. The reason for these differences is not known. Intuitively it would seem reasonable that the blunt cone boundary-layer profiles might assume a more stable shape with angle of attack, analogous to the sharp cone, and therefore cause transition to move rearward on the windward ray. Transition would not continue to move rearward, as for the sharp cone, since the effect of bluntness diminishes with angle of attack. It would be expected that the curves would turn and approach the sharp cone curve. At some larger angle of attack all of the curves should merge into a single curve.

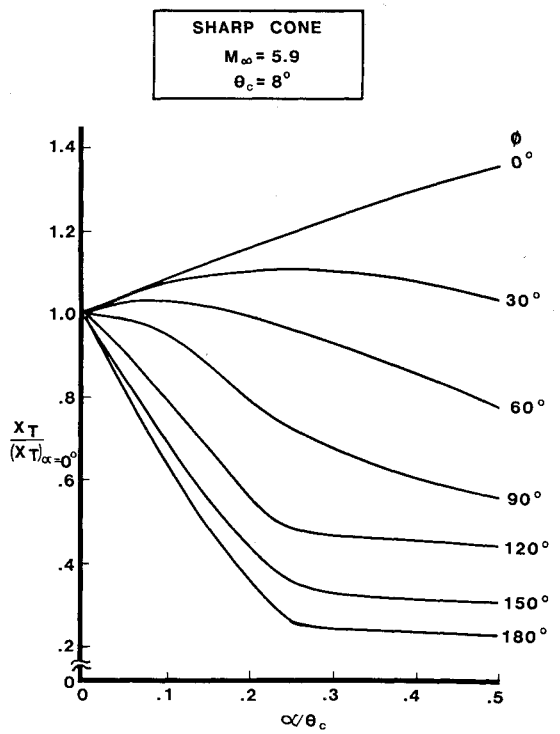

Fig. 7 Transition asymmetry with angle of attack for a sharp cone.

Figure 6 presents the transition patterns obtained for the sharp cone at $\alpha=0.5$, 1, 1.5, 2, 3, and 4 deg and $Re_\infty/\text{ft}=9.7\times10^6$. $\phi=0$ deg is the windward meridian and $\phi=180$ deg is the leeward meridian. The shaded area represents the transition region, with curve B indicating the beginning of transition and curve E the end of transition. The beginning and end of transition at $\alpha=0$ deg is shown for reference. For $\alpha=2$-and 4-deg calculated values of local Re_θ are given. These local Reynolds numbers at angle of attack were obtained from the boundary-layer code of Ref. 13. The patterns do not change significantly with increases in angle of attack. The main effect of increasing angle of attack was a continuing rearward displacement on the windward side and a forward displacement on the leeward side until a limiting displacement was obtained.

The data of Fig. 6 have been used to show the beginning of transition in a nondimensionalized format in Fig. 7. Angle-of-attack data are often presented in a nondimensionalized format such as this with the implication that the results represent universal curves. No such inference is made here since the possible influence of parameters such as Mach number, cone angle, surface roughness, wall temperature, and facility characteristics can not presently be evaluated.

Figure 8 presents the transition patterns obtained with the 5% spherically blunt nosetip ($R_N/R_B=0.05$) at $\alpha=0.5$, 1, 1.5, 2, and 4 deg and $Re_\infty/\text{ft}=19.4\times10^6$. The format of presentation is similar to that of Fig. 6. The shape of the transition regions differ from those found with the sharp tip in that most of the transition asymmetry occurs between $\phi=60$ and 120 deg. There was little change on the windward

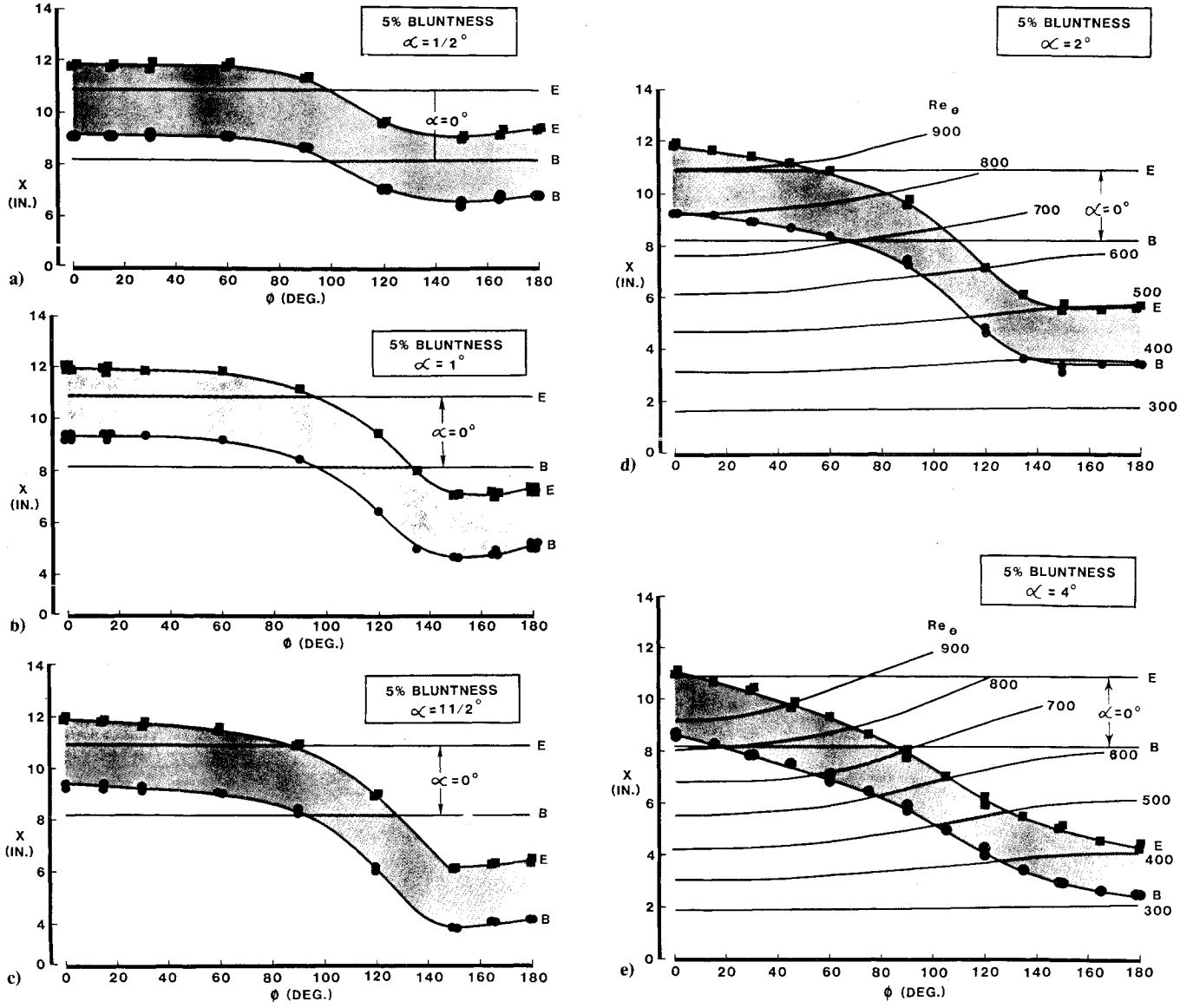

Fig. 8 Transition pattern on a cone with 5% nosetip bluntness: a) $\alpha = 1.5$ deg, b) $\alpha = 1$ deg, c) $\alpha = 1.5$ deg, d) $\alpha = 2$ deg, e) $\alpha = 4$ deg.

side between $\alpha = 0.5$ and 1.5, whereas the leeward transition front steadily moved forward.

Figure 9 presents the beginning of transition for the 5% blunt nosetip in a nondimensionalized form, similar to Fig. 7. These results have many similarities with those features found for the sharp tip, with basic differences being a limited rearward movement of transition on the windward side, a smaller overall circumferential variation in the transition pattern, and most of the circumferential variation occurring between $\phi = 60$ and 120 deg. Note that the magnitude of the transition asymmetry (displacement between $\phi = 0$ and 180 deg) is not changing greatly for $0.25 < \alpha/\theta_c < 0.50$ since the windward ray change is similar to the leeward ray.

Continuing in the same format, Fig. 10 presents the transition patterns obtained with the 10% spherically blunt nosetip ($R_N/R_B = 0.10$) at $\alpha = 0.5$, 1, 1.5, 2, and 4 deg and $Re_\infty/\text{ft} = 19.4 \times 10^6$. The patterns were found to be similar to those obtained with the 5% blunt nosetip. Transition on the windward ray at $\alpha = 2$ deg was displaced more than 2 in. farther downstream than the location obtained with the 5% blunt nosetip, yet the local transition Reynolds number was approximately 800 in both cases. Similarly, at $\alpha = 4$ deg, the transition Reynolds numbers were about the same on the

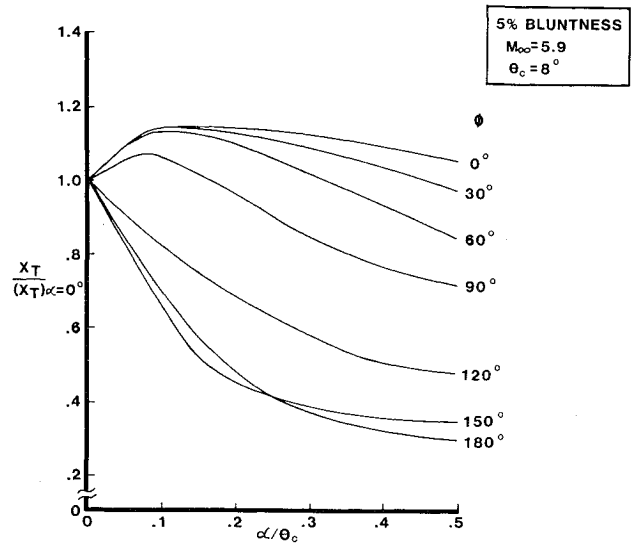

Fig. 9 Transition asymmetry with angle of attack for 5% nosetip bluntness.

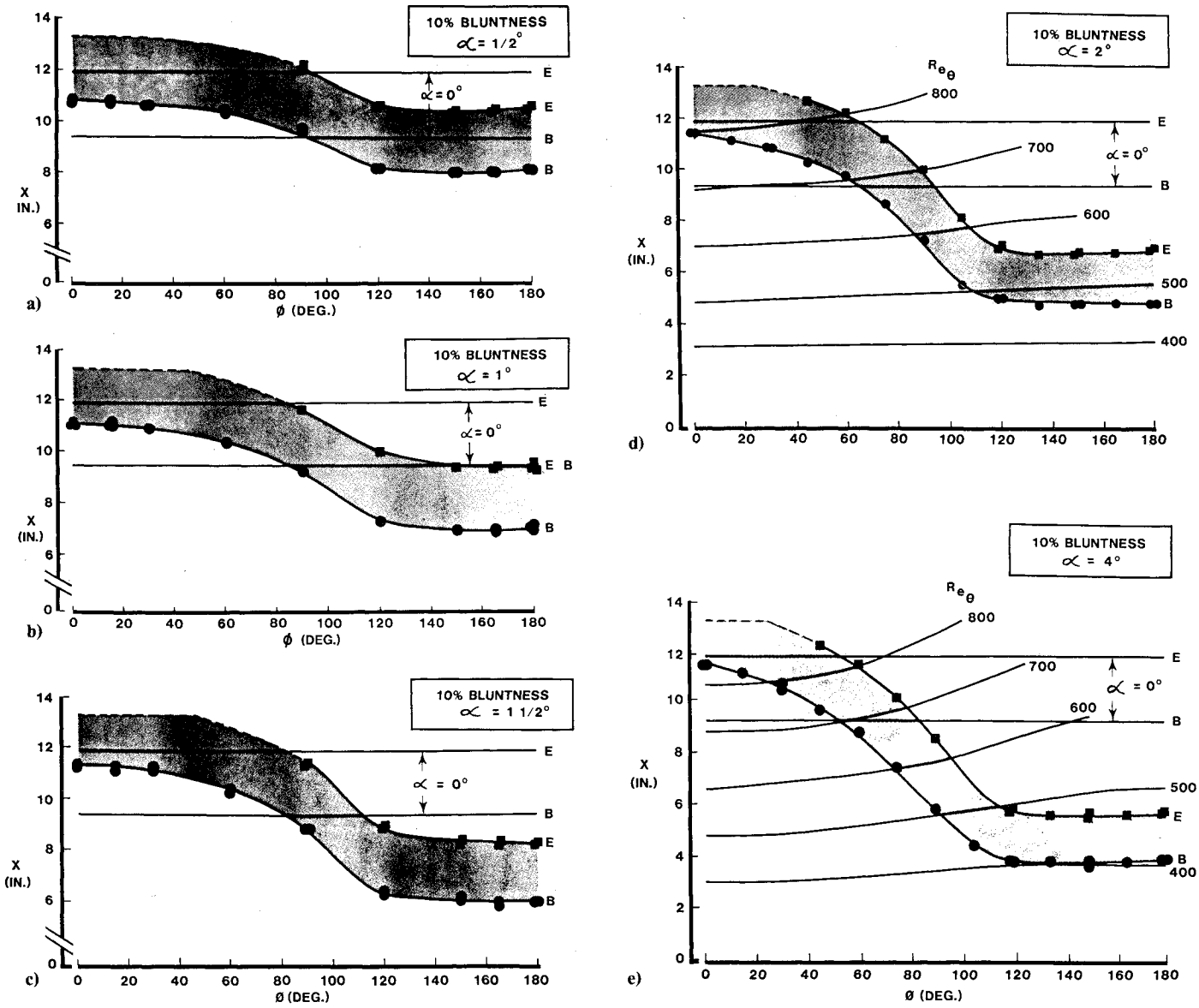

Fig. 10 Transition pattern on a cone with 10% nosetip bluntness, a) $\alpha = 0.5$ deg; b) $\alpha = 1$ deg; c) $\alpha = 1.5$ deg; d) $\alpha = 2$ deg; e) $\alpha = 4$ deg.

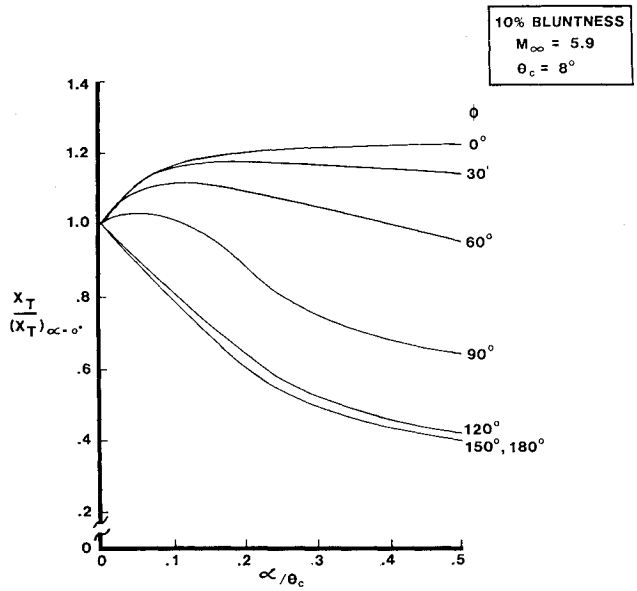

Fig. 11 Transition asymmetry with angle of attack for 10% nosetip bluntness.

windward ray for both the 5 and 10% blunt nosetips even though the transition locations were significantly different.

The beginning of transition for the cone with 10% nosetip bluntness is presented in nondimensionalized form in Fig. 11. The trends were found to be similar to those of the cone with 5% nosetip bluntness.

Figure 12 compares transition location on the windward and leeward meridians obtained with the three simulated laminar ablated nosetips with the corresponding data for spherically blunt nosetips (spherically blunt nosetip data from Fig. 5). Most of the data from the simulated laminar ablated nosetips can be explained in terms of additional blunting of the nosetip. That is, the results are representative of what would be expected with a slightly larger spherical nosetip. An exception occurs on the windward meridian of the 10%L and 15%L nosetips at angles of attack of 4 deg and larger. In this situation transition occurred somewhat earlier on the frustum than was found with the corresponding spherically blunt nosetips.

Figure 13 shows the transition pattern obtained with the 10%L nosetip at $\alpha = 2$ deg and $Re_\infty/\text{ft} = 19.4 \times 10^6$. The dotted curves are the corresponding transition results obtained with a spherically blunt nosetip at these conditions

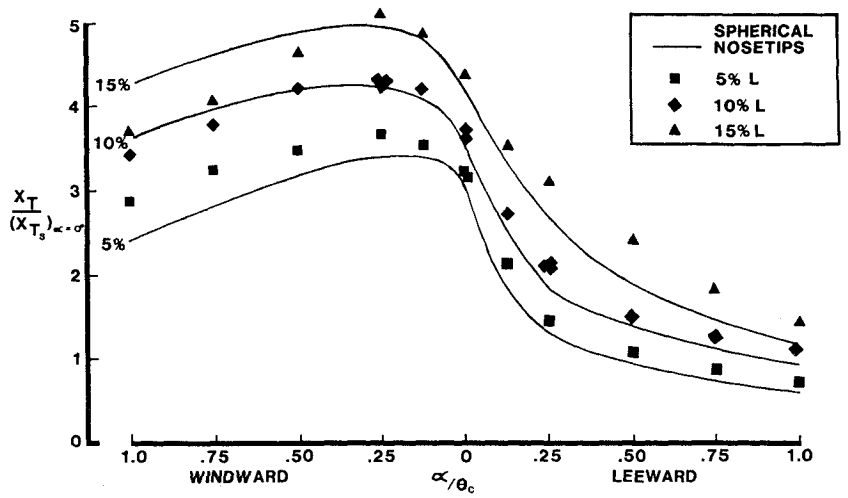

Fig. 12 Transition movement with angle of attack for simulated laminar ablated nosetips.

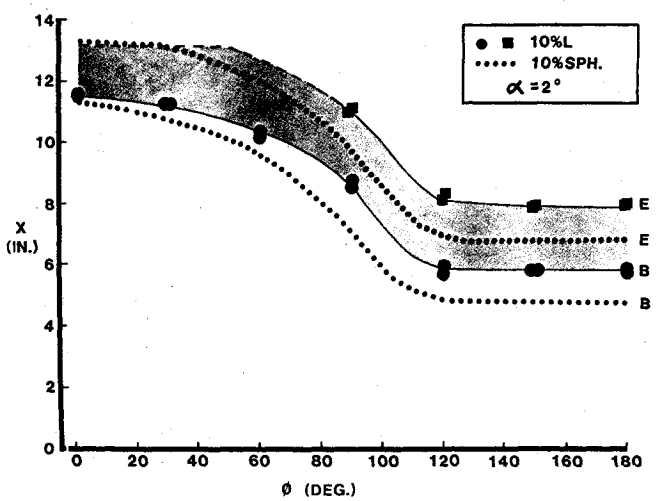

Fig. 13 Transition pattern for a cone with a 10% simulated laminar ablated nosetip, $\alpha = 2$ deg.

(spherically blunt data from Fig. 10d). The pattern was similar to that obtained with the 10% spherically blunt nosetip, with only small differences in the magnitude of transition displacement.

Conclusions

Following are the major conclusions obtained from this investigation.

1) The present data are consistent with other angle of attack transition investigations in that the general trend of sharp cone transition movement with angle of attack was a rearward movement of transition on the windward ray and a forward movement on the leeward ray.

2) Transition location was sensitive to small changes in angle of attack for both sharp and blunt tipped configurations. Small angles of attack were found to produce large asymmetries in the frustum transition pattern.

3) Most of the frustum transition asymmetry for blunt nosetips occurred between $\phi = 60$ and 120 deg.

4) Data obtained with simulated laminar ablated nosetips were generally representative of what would be expected with a larger spherically blunt nosetip.

References

[1] DiCristina, V., "Three Dimensional Laminar Boundary Transition on a Sharp 8 deg Cone at Mach 10," *AIAA Journal,* Vol. 8, May 1970, pp. 852-856.

[2] Ward, L.K., "Influence of Boundary Layer Transition on Dynamic Stability at Hypersonic Speeds," *Transactions of the Second Technical Workshop on Dynamic Stability Testing,* Vol. II, AEDC, April 1965.

[3] Holden, M.S., "Studies of the Effects of Transitional and Turbulent Boundary Layers on the Aerodynamic Performance of Hypersonic Re-Entry Vehicles in High Reynolds Number Flows," AFOSR-TR-79-0125, Dec. 1978.

[4] Krogmann, P., "An Experimental Study of Boundary Layer Transition on a Slender Cone at Mach 5," AGARD Symposium on Laminar Turbulent Transition, Technical University of Denmark, Copenhagen, Denmark, May 1977.

[5] Mateer, G.C., "Effects of Wall Cooling and Angle of Attack on Boundary Layer Transition on Sharp Cones at $M_\infty = 7.4$," NACA TN D-6908, Aug. 1972.

[6] Muir, J.F. and Trujillo, A.A., "Experimental Investigation of the Effects of Nose Bluntness, Free-Stream Unit Reynolds Number, and Angle of Attack on Cone Boundary Layer Transition at a Mach Number of 6," AIAA Paper 72-216, Jan. 1972.

[7] Stetson, K.F. and Rushton, G.H., "Shock Tunnel Investigation of Boundary Layer Transition at $M = 5.5$," *AIAA Journal,* Vol. 5, May 1967, pp. 899-906.

[8] Stetson, K.F., "Effect of Bluntness and Angle of Attack on Boundary Layer Transition on Cones and Biconic Configurations," AIAA Paper 79-0269, Jan. 1979.

[9] Stetson, K.F., "Hypersonic Boundary Layer Transition Experiments," AFWAL-TR-80-3062, Oct. 1980.

[10] Moore, F.K., "Laminar Boundary Layer on a Circular Cone in Supersonic Flow at Small Angle of Attack," NACA TN 2521, Oct. 1951.

[11] Fiore, A.W. and Law, C.H., "Aerodynamic Calibrations of the Aerospace Research Laboratories M = 6 High Reynolds Number Facility," ARL-TR-75-0028, Feb. 1975.

[12] Pate, S.R., "Dominance of Radiated Aerodynamic Noise on Boundary Layer Transition in Supersonic Hypersonic Wind Tunnels, Theory and Application," AEDC-TR-77-107, March 1978.

[13] Hecht, A.M. and Nestler, D.E., "A Three-Dimensional Boundary Layer Computer Program for Sphere-Cone Type Reentry Vehicles, Vol. 1, Engineering Analysis and Code Description," AFFDL-TR-78-67, June 1978.